



# Solar photoelectrocatalytic degradation of Acid Orange 7 azo dye using a highly stable TiO<sub>2</sub> photoanode synthesized by atmospheric plasma spray

Sergi Garcia-Segura<sup>a</sup>, Sergi Dosta<sup>b</sup>, Josep M. Guilemany<sup>b</sup>, Enric Brillas<sup>a,\*</sup>

<sup>a</sup> Laboratori d'Electroquímica dels Materials i del Medi Ambient, Departament de Química Física, Facultat de Química, Universitat de Barcelona, Martí i Franquès 1-11, 08028 Barcelona, Spain

<sup>b</sup> CPT Thermal Spray Centre, Materials Engineering, Departament d'Enginyeria Química i Metal·lúrgia, Universitat de Barcelona, Martí i Franquès 1-11, 08028 Barcelona, Spain

## ARTICLE INFO

### Article history:

Received 16 August 2012

Received in revised form

17 November 2012

Accepted 22 November 2012

Available online 1 December 2012

### Keywords:

Acid Orange 7

Photocatalysis

Photoelectrocatalysis

Sunlight

Water treatment

## ABSTRACT

A TiO<sub>2</sub> coating composed of 29% rutile, 9% anatase and 62% of Ti<sub>7</sub>O<sub>13</sub> on stainless steel support has been prepared by atmospheric plasma spray technology. This novel photoanode was coupled to an air-diffusion cathode that generates H<sub>2</sub>O<sub>2</sub> in a photoelectrochemical cell submitted to direct sunlight irradiation to degrade 100 mL of Acid Orange 7 (AO7) azo dye solutions in 0.05 M Na<sub>2</sub>SO<sub>4</sub> by solar photoelectrocatalysis (SPEC). The photoanode presented excellent mechanical properties as well as large stability and long durability up to 2.0 mA cm<sup>-2</sup>. The decolorization process in SPEC was synergistic of the individual processes in solar photocatalysis and anodic oxidation with generated H<sub>2</sub>O<sub>2</sub> under comparable conditions owing to the larger production of •OH from the higher amounts of photogenerated holes that can be separated of photogenerated electrons. The best operating variables for SPEC were 15 mg L<sup>-1</sup> AO7, pH 7.0 and anodic current density (*j*<sub>anod</sub>) of 1.0 mA cm<sup>-2</sup>. Under these conditions, the azo dye disappeared in 100 min and the solution was totally decolorized in 120 min, but only 40% mineralization was attained after 240 min of electrolysis. The AO7 decay followed a pseudo-first-order reaction as found by reversed-phase HPLC and it was accelerated with increasing *j*<sub>anod</sub> due to the higher amounts of •OH generated from the production of more photogenerated holes and the enhancement of anodic oxidation of water. Ion-exclusion HPLC allowed the identification of generated carboxylic acids like phthalic, tartaric, succinic, acetic and oxamic, which were the main components of long-time electrolysis. Their persistence explains the low mineralization of AO7 in SPEC. The initial N of the azo dye was mineralized as NH<sub>4</sub><sup>+</sup> ion, in larger proportion than NO<sub>3</sub><sup>-</sup> ion, although it was mainly loss as volatile species.

© 2012 Elsevier B.V. All rights reserved.

## 1. Introduction

Azo dyes are widely used in textile and food industries in Mt quantity and represent about 70% of the world dye production. These colored compounds contain one or more azo bonds (–N=N–) as chromophore group linked to aromatic structures with functional groups such as –OH and –SO<sub>3</sub>H, among others [1,2]. The dyeing process of textile industries produces large volumes of wastewater effluents with high dye contents, which are discharged into water bodies such as lakes and rivers. Azo dyes are very stable in the aquatic environment and usually persist under ambient conditions because they are difficultly removed in conventional wastewater treatment plants due to their high stability under sunlight and high resistance to biodegradation in aerobic conditions [3]. This contamination is dangerous not

only by the esthetic problems caused in waters, but also by the potential health and environmental risks due to the toxic, carcinogenic and mutagenic properties of azo dyes and their by-products [4–6]. To avoid their environmental problems and hazardous effects on living beings, physicochemical treatments like coagulation [7], adsorption [8] or filtration by selective membranes [9], as well as some biotreatments [10], have been applied to decolorize dyeing wastewaters. However, faster and even total decolorization of these effluents can be obtained using advanced oxidation processes (AOPs) [1,2,11]. AOPs are chemical, photochemical, photocatalytic and electrochemical techniques based on the in situ production of hydroxyl radical (•OH) as strong non-selective oxidant of organic pollutants in waters [2,12–14].

In recent years, TiO<sub>2</sub> photocatalysis (PC) has been widely used for the removal of organics, including several dyes, in waters [2,15–25]. This AOP involves the irradiation of TiO<sub>2</sub> nanoparticles, mainly crystallized in the anatase form, in colloidal suspension or deposited as a thin film on Ti by UV photons of sufficient energy

\* Corresponding author. Tel.: +34 934021223; fax: +34 934021231.

E-mail address: [brillas@ub.edu](mailto:brillas@ub.edu) (E. Brillas).

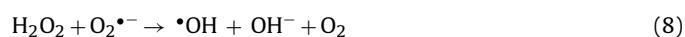
( $\lambda < 380$  nm) to promote an electron from the filled valence band to the empty conduction band ( $e_{cb}^-$ ) with an energy gap of 3.2 eV generating a positively charged vacancy or hole ( $h_{vb}^+$ ) as follows [2,18,19]:



Organics can then be either reduced by the generated electron or oxidized by the hole as well as by heterogeneous  $\bullet\text{OH}$  formed between the photogenerated vacancy and adsorbed water or  $\text{OH}^-$ :



In addition, other weaker reactive oxygen species (ROS) like superoxide radical ion ( $\text{O}_2^{\bullet-}$ ), hydroperoxyl radical ( $\text{HO}_2^\bullet$ ) and  $\text{H}_2\text{O}_2$ , as well as more  $\bullet\text{OH}$ , can be produced from the photoinjected electron by the following reactions [2,19]:



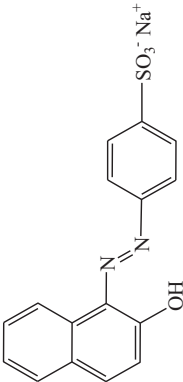
When sunlight is used as energy source, the procedure is so-called solar PC (SPC) [17,23,25]. The major loss of efficiency in PC or SPC is due to the recombination of electrons promoted to the valence band either with unreacted holes or with adsorbed hydroxyl radicals [2,12]:



Heterogeneous PC, where the  $\text{TiO}_2$  photocatalyst is immobilized onto a solid support matrix mainly by sol-gel, thermal treatment, chemical vapor deposition, electrodeposition and anodization methods, causes a loss of specific area available for photoreaction (1) and the enhancement of the electron-hole pair recombination by reaction (9) that consumes the reductive and oxidant species to destroy organics [22]. However, the efficiency of immobilized  $\text{TiO}_2$  can be strongly improved when it acts as photoanode in a photoelectrochemical system leading to the so-called photoelectrocatalysis (PEC) process under UV irradiation or solar PEC (SPEC) process under sunlight illumination [2,26–36]. These electrochemical AOPs (EAOPs) consists of the application of either a constant bias anodic potential or a low constant anodic current density ( $j_{\text{anod}}$ ) to the  $\text{TiO}_2$  photoanode subjected to illumination in order to continuously extract the photoinduced electrons by an external electrical circuit. This causes the inhibition of reactions (4)–(10) favoring the production of higher amounts of holes from reaction (1) and heterogeneous  $\bullet\text{OH}$  from reaction (2) or (3), thereby largely enhancing organics oxidation compared to PC or SPC. In PEC or SPEC, the rutile form of  $\text{TiO}_2$  immobilized onto a conductive substrate also shows significant photocatalytic oxidative efficiency, although lower than that of the anatase form [26,28,35].

In this paper, we report the synthesis of a novel  $\text{TiO}_2$  photoanode from the deposition of a  $\text{TiO}_2$  coating on a stainless steel substrate using the atmospheric plasma spray (APS) technology [37–39]. This photoanode presented excellent mechanical properties and long durability to the pass of relatively high  $j_{\text{anod}}$  values in SPEC. Its oxidation ability on azo dyes was tested in a photoelectrochemical reactor under direct solar irradiation by studying the decolorization and degradation of Acid Orange 7 (AO7 or Orange II, see formula and characteristics in Table 1) as representative model compound, since it is non-biodegradable and commonly used in

**Table 1**  
Chemical structure and characteristics of Acid Orange 7 azo dye.

Chemical structure	Chemical formula	Color index name	Chemical name	Color index number	$\lambda_{\text{max}}/\text{nm}$	$M/\text{g mol}^{-1}$
	$\text{NaC}_{16}\text{H}_{10}\text{N}_2\text{O}_4\text{S}$	Acid Orange 7 (AO7)	Sodium 4-[(2E)-2-(2-oxonaphthalen-1-ylidene)hydrazinyl] benzenesulfonate	15510	484	350.32

textile industries. The degradation of AO7 by PC [15] and SPC [16] with  $\text{TiO}_2$  in suspension, as well as by PEC with UVA light and SPEC with  $\text{TiO}_2$  deposited on transparent conducting substrates [31], has been reported. Note that azo dyes can be reduced at the cathode of an electrochemical and photoelectrochemical system, depending on the nature of the cathodic material [2]. For this reason and to avoid the possible competitive cathodic reduction of AO7 and its intermediates, a carbon-polytetrafluoroethylene (PTFE) air-diffusion cathode was chosen in the present work since it inhibits organic reduction because efficiently generates  $\text{H}_2\text{O}_2$  from injected  $\text{O}_2$  as follows [40–43]:



The comparative decolorization efficiency for AO7 solutions using SPC, electrochemical oxidation or anodic oxidation with generated  $\text{H}_2\text{O}_2$  (AO- $\text{H}_2\text{O}_2$ ) and SPEC was examined. The best operating variables like pH, dye content and applied  $j_{\text{anod}}$  for the decolorization process in SPEC were determined. The decay kinetics for AO7 and the evolution of generated carboxylic acids and released inorganic nitrogen ions were followed by chromatographic techniques.

## 2. Experimental

### 2.1. Chemicals

Pure AO7 azo dye was purchased from Acros Organics and used as received. Phthalic, tartaric, succinic, oxamic and acetic acids were of analytical grade from Panreac and Avocado. Anhydrous sodium sulphate used as background electrolyte was of analytical grade from Fluka. Synthetic dye solutions were prepared with high-purity water obtained from a Millipore Milli-Q system with resistivity  $>18 \text{ M}\Omega \text{ cm}$  at  $25^\circ\text{C}$  and their pH was adjusted with either analytical grade sulphuric acid or analytical sodium hydroxide, both supplied by Merck. Organic solvents and other chemicals employed were of either HPLC or analytical grade from Merck, Fluka and Sigma-Aldrich.

### 2.2. Preparation of $\text{TiO}_2$ coating onto stainless steel by APS

$\text{TiO}_2$  powder supplied by Sulzer Metco was used as feedstock to synthesize the final coating onto stainless steel by APS technology using an F4 plasma torch with a Sultzer Metco A-3000S system. APS consists of heating up, mixing and homogenization of the feedstock powder particles during their short residence time in the hot zone of the plasma jet. The molten droplets are then accelerated and quenched onto the substrate to produce the coating layer by layer [37–39]. A flat 316L stainless steel ( $50 \text{ mm} \times 30 \text{ mm} \times 5 \text{ mm}$ ) was used as substrate, which was previously degreased with acetone and grit blasted with white corundum at 5.6 bar and  $45^\circ$  using a blasting distance of 250 mm. The grit blasted substrate had a mean roughness ( $R_a$ ) of about  $5 \mu\text{m}$ . The spraying parameters for the  $\text{TiO}_2$  coating were taken within the following intervals: argon flow plasma ( $20\text{--}40 \text{ L min}^{-1}$ ), hydrogen flow plasma ( $10\text{--}15 \text{ L min}^{-1}$ ), applied current ( $550\text{--}650 \text{ A}$ ), spray distance ( $80\text{--}160 \text{ mm}$ ) and feed rate ( $10\text{--}30 \text{ g min}^{-1}$ ).

### 2.3. SPC, AO- $\text{H}_2\text{O}_2$ and SPEC systems

Fig. 1 illustrates a sketch of the set-up used for the SPEC degradation of 100 mL of AO7 solutions. The photoelectrochemical reactor was an undivided, open and cylindrical cell with a double jacket in which external water circulated to maintain the solution temperature at  $35^\circ\text{C}$  using a Thermo Electron Corporation HAAKE DC 10 thermostat. This temperature was chosen because it is the

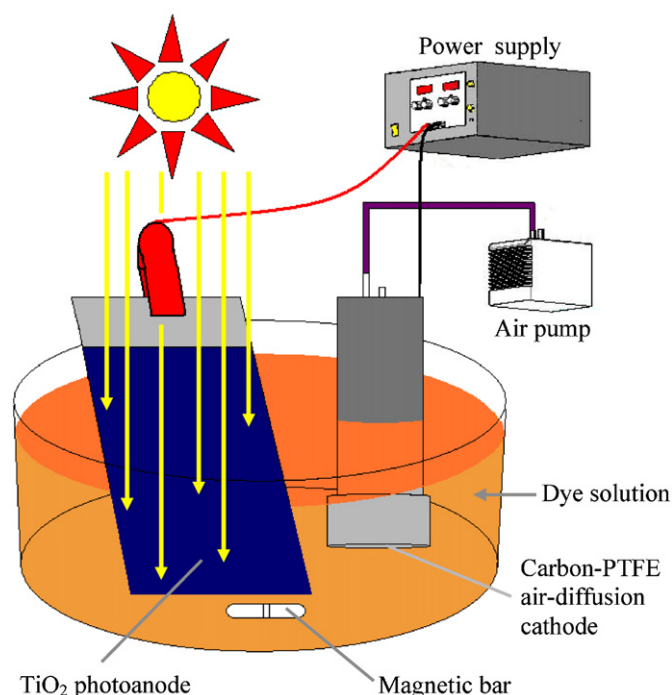


**Fig. 1.** Sketch of the experimental set-up used for the degradation of 100 mL of Acid Orange 7 (AO7) solutions by solar photoelectrocatalysis (SPEC). The photoelectrochemical reactor contained a  $\text{TiO}_2$  photoanode of  $5 \text{ cm}^2$  area, which was prepared by  $\text{TiO}_2$  deposition on a stainless steel substrate by atmospheric plasma spray technology. The air-diffusion cathode of  $3 \text{ cm}^2$  area supplied continuously  $\text{H}_2\text{O}_2$  to the dye solution from  $\text{O}_2$  reduction. The solution was thermostated at  $35^\circ\text{C}$ .

maximum value allowed in the reactor with insignificant water evaporation during prolonged treatment. The photoanode was the above-synthesized  $\text{TiO}_2$  electrode with  $5 \text{ cm}^2$  area, whereas the cathode was a  $3 \text{ cm}^2$  carbon-PTFE air-diffusion electrode supplied by E-TEK and mounted as described elsewhere [44]. This cathode was fed with air pumped at  $300 \text{ mL min}^{-1}$  to generate  $\text{H}_2\text{O}_2$  from reaction (11) and the interelectrode gap was about 1 cm. The electrochemical assays were performed at constant  $j_{\text{anod}}$  provided with an Amel 2053 potentiostat-galvanostat. The same system was used for the experiments of AO- $\text{H}_2\text{O}_2$  in the dark and SPC without pass of current. Prior to the electrolytic trials, the air-diffusion cathode was activated by polarization in  $0.05 \text{ M Na}_2\text{SO}_4$  using the same reactor with a  $3 \text{ cm}^2$  Pt anode at  $j_{\text{anod}} = 100 \text{ mA cm}^{-2}$  for 60 min. All experiments were carried out under vigorous stirring with a magnetic bar at 800 rpm to ensure homogenization and the transport of reactants towards/from the  $\text{TiO}_2$  electrode or photocatalyst.

In the SPC and SPEC trials, the immersed  $\text{TiO}_2$  photocatalyst was tilted  $41^\circ$  from the solution surface to better collect the direct sun rays in our laboratory of Barcelona (latitude:  $41^\circ 21' \text{N}$ , longitude:  $2^\circ 10' \text{E}$ ). Solar assays were made for 300 min as maximal in sunny and clear days during the summer of 2011, with similar average UV irradiation intensities between 300 and  $400 \text{ nm}$  of  $30.3$  and  $31.2 \text{ W m}^{-2}$ , as measured with a Kipp & Zonen CUV 5 radiometer.

All SPC, AO- $\text{H}_2\text{O}_2$  and SPEC experiments were made with solutions containing  $0.05 \text{ M Na}_2\text{SO}_4$  as background electrolyte. This environmentally friendly medium was chosen because it is usually employed in electrochemical systems to clarify the oxidation role of generated  $\cdot\text{OH}$  radicals [2]. The best conditions for AO7 decolorization in SPEC were found by studying the effect of pH between 3.0 and 11.0, azo dye concentration up to  $45 \text{ mg L}^{-1}$  and  $j_{\text{anod}}$  up to  $2.0 \text{ mA cm}^{-2}$ .

## 2.4. Apparatus and analytical procedures

The particle size distribution of the feedstock TiO<sub>2</sub> powder was measured by laser scattering using a Beckman Coulter LS equipment. Scanning electron microscopy (SEM) images of the initial and deposited TiO<sub>2</sub> were obtained using a Jeol 5510 system, which was coupled with an energy dispersive X-ray spectrometry (EDS) phase analyzer from Röntec. More accurate phase analysis of the starting powder and coating was performed by X-ray diffractometry (XRD) using a Siemens D500 system type Bragg-Brentano  $\theta/\theta$  by applying a Cu K $\alpha_{1+2}$  radiation ( $\lambda(\alpha_1)=0.154060$  nm and  $\lambda(\alpha_2)=0.154443$  nm) at 40 kV and 30 mA current. The ratio between the obtained crystalline phases was calculated from their reference intensity ratio (RIR) by the Chung's method [45] and applying the X'pert HighScore Plus software. The porosity of the coating was measured with a Matrox Inspector software image analyzer. Its microroughness was determined with a Mitutoyo Surftest 301 equipment and its adhesion was measured with a Servosis MCH-102ME system through the ASTM C633 standard. Cross-sectional microhardness measurements were performed with a Matsuzawa MXT- $\alpha$  system by Vickers indentation at 300 g load using the UNE 7-423/2 standard. Indentations were determined with a Leica DMI 5000 M optical microscope to increase their accuracy.

The pH of AO7 solutions was measured with a Crison GLP 22 pH-meter. Before analysis, the aliquots were filtered with 0.45  $\mu$ m PTFE filters from Whatman. The decolorization process of azo dye solutions in SPC, AO-H<sub>2</sub>O<sub>2</sub> and SPEC was monitored from the decay of the absorbance (*A*) at the maximum wavelength ( $\lambda_{\text{max}}=484$  nm) of AO7 (see Table 1), measured on the spectra recorded with a Shimadzu 1800 UV–vis spectrophotometer at 35 °C. The percentage of color removal or decolorization efficiency was then calculated from the following equation [42,43]:

$$\% \text{Color removal} = \frac{A_0 - A_t}{A_0} 100 \quad (12)$$

where *A*<sub>0</sub> and *A* are the absorbance at initial time and time *t* at the  $\lambda_{\text{max}}$  of the azo dye, respectively.

The concentration of accumulated H<sub>2</sub>O<sub>2</sub> was determined from the light absorption of its Ti(IV) colored complex at  $\lambda=409$  nm [46] using the above spectrophotometer thermostated at 35 °C. The mineralization of azo dye solutions was determined from the abatement of their TOC, measured on a Shimadzu VCSN analyzer. Reproducible TOC values with an accuracy of  $\pm 1\%$  were obtained by injecting 50  $\mu$ L aliquots to the analyzer. Total nitrogen (TN) was determined with a Shimadzu TNM-1 unit coupled to the above TOC analyzer.

The decay of AO7 concentration in SPEC was followed by reversed-phase HPLC using a Waters 600 LC fitted with a Spherisorb ODS2 5  $\mu$ m (150 mm  $\times$  4.6 mm) column at 35 °C and coupled to a Waters 996 photodiode array detector selected at the  $\lambda_{\text{max}}$  of the azo dye. Generated carboxylic acids in SPEC were detected by ion-exclusion HPLC using the above LC fitted with a Bio-Rad Aminex HPX 87H (300 mm  $\times$  7.8 mm) column at 35 °C and the photodiode array detector set at  $\lambda=210$  nm. For these measurements, 20  $\mu$ L aliquots were injected into the LC and the mobile phase was either a 30:70 (v/v) acetonitrile/water mixture with 2.4 mM *n*-butylamine at 0.6 mL min<sup>−1</sup> for reversed-phase HPLC or 4 mM H<sub>2</sub>SO<sub>4</sub> at 0.6 mL min<sup>−1</sup> for ion-exclusion HPLC. The inorganic nitrogen ions released in SPEC treatment were quantified by ionic chromatography with a Shimadzu 10 Avp HPLC coupled with a Shimadzu CDD 10 Avp conductivity detector. The NH<sub>4</sub><sup>+</sup> concentration was determined with a Shodex IC YK-421 (125 mm  $\times$  4.6 mm) cation column at 40 °C under circulation of a 5.0 mM tartaric acid, 1.0 mM dipicolinic acid, 24.2 mM boric acid and 1.5 mM crown ether solution at 1.0 mL min<sup>−1</sup> as mobile

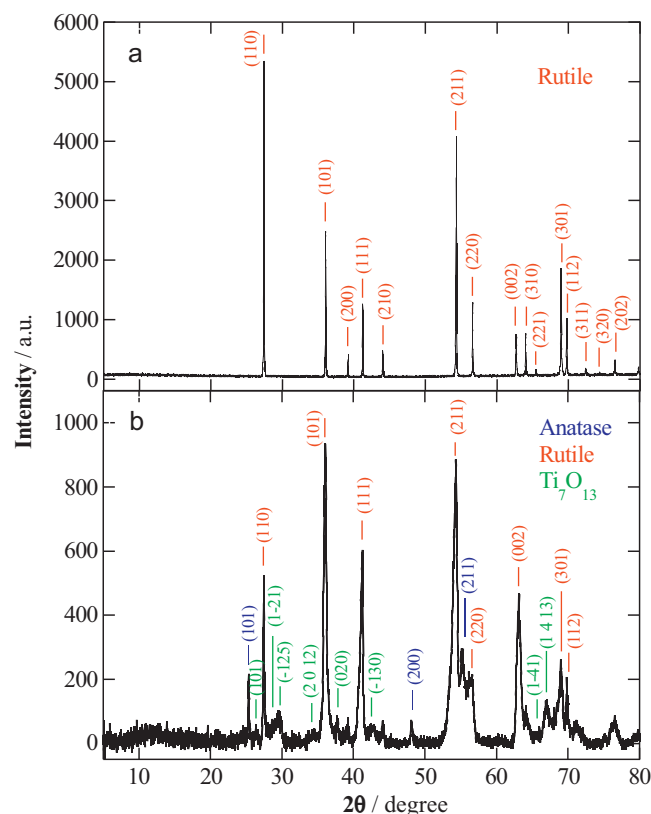


**Fig. 2.** X-ray diffractograms of (a) the semiconductor TiO<sub>2</sub> powder composed of 100% rutile and (b) the prepared TiO<sub>2</sub> photoanode by atmospheric plasma spray technology composed of 29% rutile, 9% anatase and 62% of non-stoichiometric phase of Ti<sub>7</sub>O<sub>13</sub>. The corresponding crystallographic planes for each phase are assigned.

phase. The NO<sub>3</sub><sup>−</sup> content was obtained with a Shim-Pack IC-A15 (100 mm  $\times$  4.6 mm) anion column at 40 °C using a mobile phase of 2.4 mM tris(hydroxymethyl)aminomethane and 2.5 mM phthalic acid of pH 4.0 at 1.5 mL min<sup>−1</sup>.

## 3. Results and discussion

### 3.1. Characterization of the TiO<sub>2</sub> coating prepared by APS

Figs. 2 and 3 depict the X-ray diffractograms and SEM images obtained for both, the TiO<sub>2</sub> feedstock powder and the resulting coating by APS, respectively. As can be seen in Fig. 2a, the starting powder prepared by a sintering and crushing process was only composed of rutile phase [47]. The SEM image of Fig. 3a shows that the free-surface of the initial powder exhibited an irregular blocky morphology only composed of TiO<sub>2</sub> microparticles, also corroborated by its EDS analysis. The particle size distribution of this powder measured by laser scattering ranged between 20 and 50  $\mu$ m, with a mean particle size of 32  $\mu$ m.

Fig. 2b shows the XRD pattern for the TiO<sub>2</sub> coating on stainless steel. Crystallographic planes related to the rutile [47] and anatase [48] forms, along with those ascribed to a non-stoichiometric Ti<sub>7</sub>O<sub>13</sub> [49], are also given in Fig. 2b to show that a part of the initial rutile is conserved, but another part of it is transformed into anatase and Ti<sub>7</sub>O<sub>13</sub> under APS deposition. Moreover, the peaks for the TiO<sub>2</sub> coating were wider than those of pure compounds due to formation of the non-stoichiometric phase and a grain size reduction, as typically found for coatings obtained by APS. Analysis of the crystallographic phases revealed that the 100% rutile-TiO<sub>2</sub> phase powder was converted after the APS process into a coating containing 29% of rutile, 9% of anatase and 62%



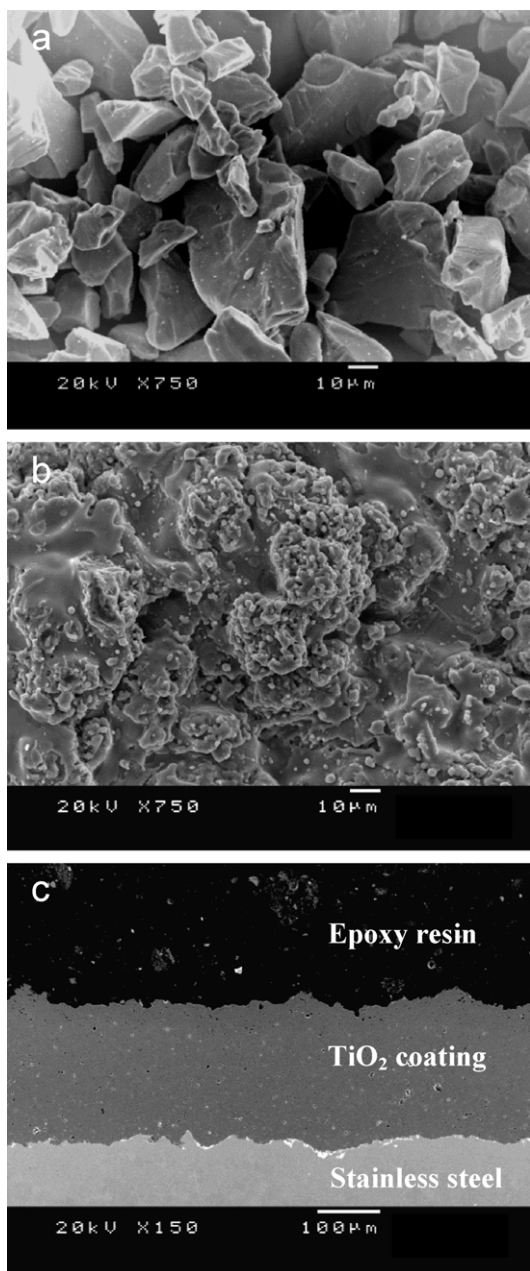


**Fig. 3.** Scanning electron microscopy (SEM) images of (a) the free-surface micrograph of the initial  $\text{TiO}_2$  powder, (b) the free-surface micrograph of the microparticulated  $\text{TiO}_2$  coating prepared by atmospheric plasma spray and (c) the cross section of the  $\text{TiO}_2$  coating on stainless steel substrate.

of  $\text{Ti}_7\text{O}_{13}$ . An anatase-to-rutile ratio of 0.31 was then formed at the coating. The SEM image of Fig. 3b of its free surface also confirms that some microparticles were fully melted during the APS process. The excellent deposition obtained by this technique can be observed in the SEM cross-section of Fig. 3c, showing a homogeneous microstructure with a thickness of  $211 \pm 21 \mu\text{m}$ . It was found that its porosity was of  $4.0 \pm 1.7\%$ , with a microroughness of  $8.1 \pm 1.5 \mu\text{m}$ . Moreover, the adhesion of the coating was  $39.8 \pm 3.8 \text{ MPa}$  and its HVN microhardness was  $842 \pm 28$ . The coating failed by the substrate interface after the C633 adhesion test.

The  $\text{TiO}_2$  coating on stainless steel synthesized by APS then presented excellent mechanical properties and also showed large stability and long durability to the current pass. Thus, using the SPEC system of Fig. 1 with 100 mL of 0.05 M  $\text{Na}_2\text{SO}_4$  as background

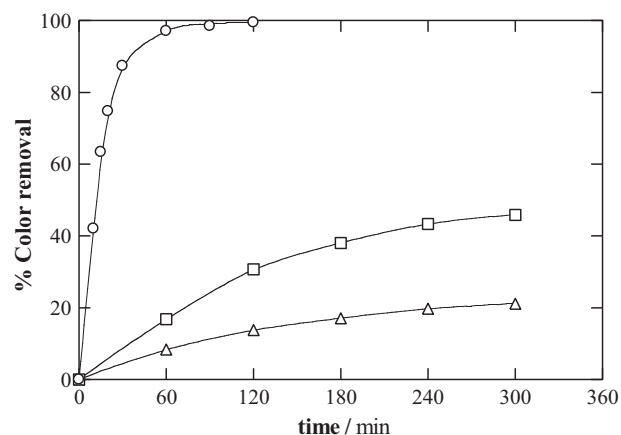


**Fig. 4.** Variation of percentage of color removal with time for the treatment of 100 mL of a  $15 \text{ mg L}^{-1}$  AO7 solution in 0.05 M  $\text{Na}_2\text{SO}_4$  at pH 7.0 and  $35^\circ\text{C}$ . ( $\Delta$ ) Solar photocatalysis (SPC) with the synthesized  $\text{TiO}_2$  coating, ( $\square$ ) anodic oxidation with generated  $\text{H}_2\text{O}_2$  (AO- $\text{H}_2\text{O}_2$ ) using the  $\text{TiO}_2$ /air-diffusion cell at anodic current density ( $j_{\text{anod}}$ ) of  $1.0 \text{ mA cm}^{-2}$  in the dark and ( $\circ$ ) SPEC under the same conditions but exposing the photoelectrochemical cell directly to sunlight.

electrolyte, no change in the characteristics of the  $\text{TiO}_2$  photoanode was found operating up to  $j_{\text{anod}} = 2.0 \text{ mA cm}^{-2}$ , where a bias anodic potential of about 1.75 V vs SCE was attained. This anodic current density was chosen as maximal for the AO- $\text{H}_2\text{O}_2$  and SPEC trials performed with this electrode. All experiments reported below were comparatively made with the same  $\text{TiO}_2$  deposit.

### 3.2. Comparative color removal of AO7 solutions by SPC, AO- $\text{H}_2\text{O}_2$ and SPEC

The comparative oxidation ability of SPC, AO- $\text{H}_2\text{O}_2$  and SPEC on AO7 solutions was clarified from their corresponding decolorization efficiencies, which are typically used to check the effectiveness of an azo dye treatment. Fig. 4 illustrates the color removal obtained for  $15 \text{ mg L}^{-1}$  AO7 in 0.05 M  $\text{Na}_2\text{SO}_4$  of pH 7.0 under the application of these processes using the synthesized  $\text{TiO}_2$  photocatalyst. For AO- $\text{H}_2\text{O}_2$  and SPEC, a  $j_{\text{anod}} = 1.0 \text{ mA cm}^{-2}$  (bias anodic potential of about 1.35 V vs SCE) was applied. In all these trials, the solution pH remained practically unchanged.

As can be seen in Fig. 4, the slowest decolorization took place in SPC, where only 21% color removal was achieved in 300 min. The low effectiveness of this procedure can be associated with the fast recombination of the photogenerated oxidizing holes and reducing electrons by reaction (9), then being largely inhibited the reaction of holes with water to form  $\bullet\text{OH}$  from reaction (2), which is the main oxidant of organics at neutral pH [17,19]. Fig. 4 shows that AO- $\text{H}_2\text{O}_2$  in the dark decolorized more quickly the azo dye solution, leading to 46% color removal in 300 min. The destruction of AO7 in this method can be ascribed to the action of heterogeneous  $\bullet\text{OH}$  generated at the  $\text{TiO}_2$  anode surface as intermediate of the anodic oxidation of water to  $\text{O}_2$  by the following reaction [2,50]:



The slow decolorization found in AO- $\text{H}_2\text{O}_2$  can then be accounted by the expected small production of reactive  $\bullet\text{OH}$  on  $\text{TiO}_2$  anode from reaction (13), which is pH independent [50]. In contrast, Fig. 4 evidences that the AO7 solution was very quickly discolored, with total color removal in about 120 min, using SPEC. This behavior indicates that the application of a current allows a very effective separation of the electron-hole pair formed from reaction (1) on the  $\text{TiO}_2$  photoanode subjected to sunlight illumination, being the electrons driven to the cathode and strongly enhancing the reaction (2) between holes and water to produce large quantities of oxidant

•OH that destroy AO7 and its by-products [35]. Results of Fig. 4 confirm that the SPEC process is synergistic, but not cumulative of the individual processes, because when total color removal is attained at 120 min of SPEC, only 45% decolorization efficiency is achieved from the sum of both SPC and AO-H<sub>2</sub>O<sub>2</sub> treatments.

Note that H<sub>2</sub>O<sub>2</sub> formed at the cathode from reaction (11) was accumulated in large extent in the solution during the AO-H<sub>2</sub>O<sub>2</sub> and SPEC trials. A blank experiment was performed by adding 10 mM H<sub>2</sub>O<sub>2</sub> to 100 mL of 15 mg L<sup>-1</sup> AO7 in 0.05 M Na<sub>2</sub>SO<sub>4</sub> adjusted to pH 7.0, but no significant decolorization of this solution was found after 60 min of solar illumination, indicating that H<sub>2</sub>O<sub>2</sub> does not oxidize the azo dye. After 180 min of SPEC at  $j_{\text{anod}} = 1.0 \text{ mA cm}^{-2}$ , 1.66 mM of H<sub>2</sub>O<sub>2</sub> were detected in solution, a value lower than 2.76 mM expected from reaction (11) assuming 100% current efficiency for H<sub>2</sub>O<sub>2</sub> production. This decay in accumulated H<sub>2</sub>O<sub>2</sub> may be related to its slow reaction with photogenerated electrons from reaction (7), but it can be more probably due to its oxidation to O<sub>2</sub> at the TiO<sub>2</sub> photoanode giving rise to the weaker oxidant HO<sub>2</sub>• as follows [2]:



Reaction (14) is also expected in AO-H<sub>2</sub>O<sub>2</sub>, but the low decolorization rate found for this process (see Fig. 4) suggests a small participation of HO<sub>2</sub>• in azo dye removal.

The above results indicate that the SPEC process with the TiO<sub>2</sub> photoanode synthesized by APS is very effective for AO7 decolorization. The influence of variables like pH, azo dye concentration and  $j_{\text{anod}}$  on this EAOP was then examined to clarify the best experimental decolorization conditions, as will be discussed in subsections below.

### 3.3. Effect of pH on the AO7 decolorization in SPEC process

The change of percentage of color removal with electrolysis time for 15 mg L<sup>-1</sup> AO7 solutions in the pH range 3.0–11.0 by using SPEC at  $j_{\text{anod}} = 1.0 \text{ mA cm}^{-2}$  for 180 min as maximal is depicted in Fig. 5a. In these trials, no significant change of solution pH with electrolysis time was detected. As can be seen, complete decolorization was only feasible after 120 min of electrolysis at neutral pH 7.0, which is the optimum pH for this treatment. A similar color removal rate to pH 7.0 was also determined during the first 60 min at pH 9.0, reaching 96% decolorization, but prolonging the electrolysis the absorbance at  $\lambda = 484 \text{ nm}$  rose gradually decreasing the color decay to 68% at 180 min. The same behavior, with maximum color removal of 80% and 40% at 60 min, was also found for pH 5.0 and 11.0, respectively. A different trend can be observed in Fig. 5a for pH 3.0, where the solution was progressively decolorized, but only attaining 65% color removal in 180 min.

The complex effect of pH shown in Fig. 5a is difficult to justify from the change in the electrostatic interactions between the azo dye and the amphoteric TiO<sub>2</sub> surface [19,21], because the former is always charged negatively due to its sulfonic group while the TiO<sub>2</sub> photocatalyst is always subjected to a positive charge in SPEC. The variation of AO7 decolorization with pH can be rather related to the change of the oxidation ability of the photogenerated holes [19] and the different products formed from azo dye degradation. Thus, the removal of AO7 followed by the progressive formation of products that present a high residual absorbance at 484 nm can explain the volcano shape of the decolorization curves at pH 5.0, 9.0 and 11.0 shown in Fig. 5a, as can be deduced from the UV-Vis spectra recorded for the final treated solutions and presented in Fig. 5b.

In aqueous solution, AO7 presents two tautomeric forms in equilibrium, the azo form (see Table 1) and the hydrazone one, where the hydroxyl group appears as carbonyl group being its hydrogen linked to the azo group [16]. The hydrazone form is the major

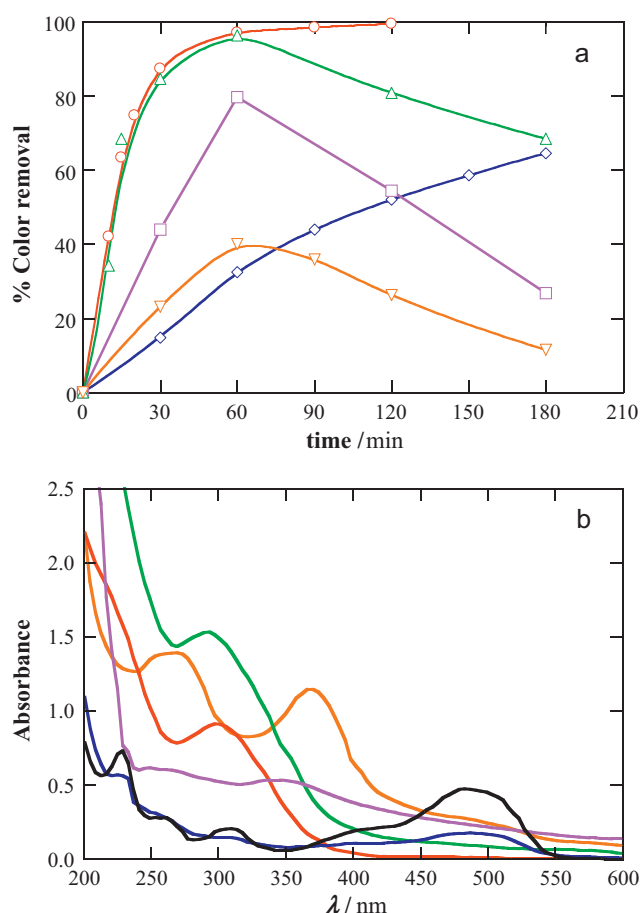


**Fig. 5.** (a) Effect of pH on the change of percentage of color removal with time for the SPEC treatment of 100 mL of solutions containing 15 mg L<sup>-1</sup> of AO7 in 0.05 M Na<sub>2</sub>SO<sub>4</sub> at  $j_{\text{anod}} = 1.0 \text{ mA cm}^{-2}$  and 35 °C. Solution pH: (◇) 3.0, (□) 5.0, (○) 7.0, (Δ) 9.0 and (▽) 11.0. (b) UV-vis spectra of the initial solution (in black) at pH 7.0 and the above final treated solutions after further adjustment to pH 7.0.

species giving a strong visible band with  $\lambda_{\text{max}} = 484 \text{ nm}$  (characteristic of AO7), whereas the azo form yields a much weaker shoulder near 430 nm. These bands can be observed in the UV-vis spectrum of the initial 15 mg L<sup>-1</sup> AO7 solution of pH 7.0 depicted in Fig. 5b, along with two other bands in the ultraviolet region centred at 230 and 305 nm due to the benzene and naphthalene groups of AO7, respectively [16]. The same four bands with analogous intensity were detected for all initial solutions in the pH range 3.0–11.0, indicating the presence of the two forms of AO7 in all them and in similar proportion. During the SPEC treatment, the bands of the two forms of AO7 were always reduced at similar rate up to disappear, except for pH 3.0 where they still persisted at 180 min (see Fig. 5b). The slower oxidation of AO7 found at pH 3.0 suggests that in this medium, organics are predominantly destroyed by photogenerated holes from reaction (1), which are weaker oxidizing agents than •OH [19]. In contrast, at higher pH the holes produce large amounts of •OH, from reaction (2) at pH 5.0 and 7.0 and/or from reaction (3) at pH 9.0 and 11.0, removing much more rapidly AO7, but giving different products depending on pH as a result of its non-selective attack on organics. Thus, Fig. 5b shows a strong band at 300 nm, related to naphthalenic derivatives, in the final solution of pH 7.0, without any absorbance for  $\lambda > 400 \text{ nm}$ . A similar strong band can be observed for pH 9.0, but with residual absorbance in the visible region probably due to the formation of low amounts of colored aromatic intermediates, thus avoiding the total decolorization of solution. A significant absorbance in the visible region was also found at pH 5.0 and 11.0, although in the latter medium

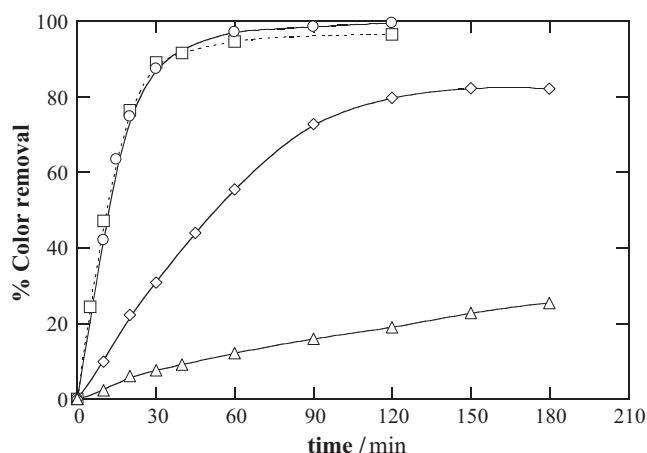


**Fig. 6.** Influence of dye concentration on the decolorization rate for 100 mL of AO7 solutions in 0.05 M Na<sub>2</sub>SO<sub>4</sub> at pH 7.0 by SPEC at  $j_{\text{anod}} = 1.0 \text{ mA cm}^{-2}$  and 35 °C. Dye concentration: (□) 5 mg L<sup>-1</sup>, (○) 15 mg L<sup>-1</sup>, (◇) 30 mg L<sup>-1</sup> and (△) 45 mg L<sup>-1</sup>.

two other bands at 263 and 365 nm due to the formation of other products were detected. The progressive increase of the residual absorbance at 484 nm after 60 min of SPEC at pH 5.0, 9.0 and 11.0 explains the volcano shape with gradual decay in color removal shown in Fig. 5a.

#### 3.4. Influence of azo dye concentration on its decolorization in SPEC process

The effect of initial AO7 concentration on color removal in SPEC was tested at the optimum neutral pH 7.0 and applying  $1.0 \text{ mA cm}^{-2}$ . Under these conditions, a maximum content of  $45 \text{ mg L}^{-1}$  was studied because of the limited oxidation ability of this method for higher azo dye concentrations. The decolorization efficiency-time plots thus obtained are presented in Fig. 6. A similar decay of the percentage of color removal for 5 and 15 mg L<sup>-1</sup> of the azo dye can be observed giving rise to total decolorization in about 120 min. However, further increase of AO7 concentration resulted in a gradual loss in color removal, reaching 82% and only 25% decolorization after 180 min of electrolysis for 30 and 45 mg L<sup>-1</sup>. Under these conditions, the disappearance of the strong band at  $\lambda_{\text{max}} = 484 \text{ nm}$  of the azo dye became progressively slower and a more rapid raise of the residual absorbance in the visible region due to colored intermediates was detected. This behavior can be mainly associated with the increasing consumption of generated •OH to oxidize the greater amounts of organics formed on the TiO<sub>2</sub> photoanode surface, thereby decreasing the amount of this radical to attack the azo dye [33,34]. Moreover, the transparency of the solution decreases at greater AO7 concentration because UV irradiation of sunlight is more strongly absorbed by the azo dye and its aromatic products yielding lower photogeneration of holes with the consequent loss of •OH production that decreases the oxidation ability of SPEC [27]. Results of Fig. 6 evidence that SPEC is able to completely decolorize solutions of pH 7.0 containing low AO7 contents up to 15 mg L<sup>-1</sup>, which can be taken as the best concentration for this treatment.

#### 3.5. Effect of anodic current density on decolorization and decay kinetics of AO7 in SPEC process

The applied  $j_{\text{anod}}$  is a key parameter in SPEC because it limits the separation of photogenerated holes and electrons and hence, the oxidation action of the former on the organic matter. The influence of this variable on AO7 decolorization was checked for a solution containing the best content of  $15 \text{ mg L}^{-1}$  of azo dye at the

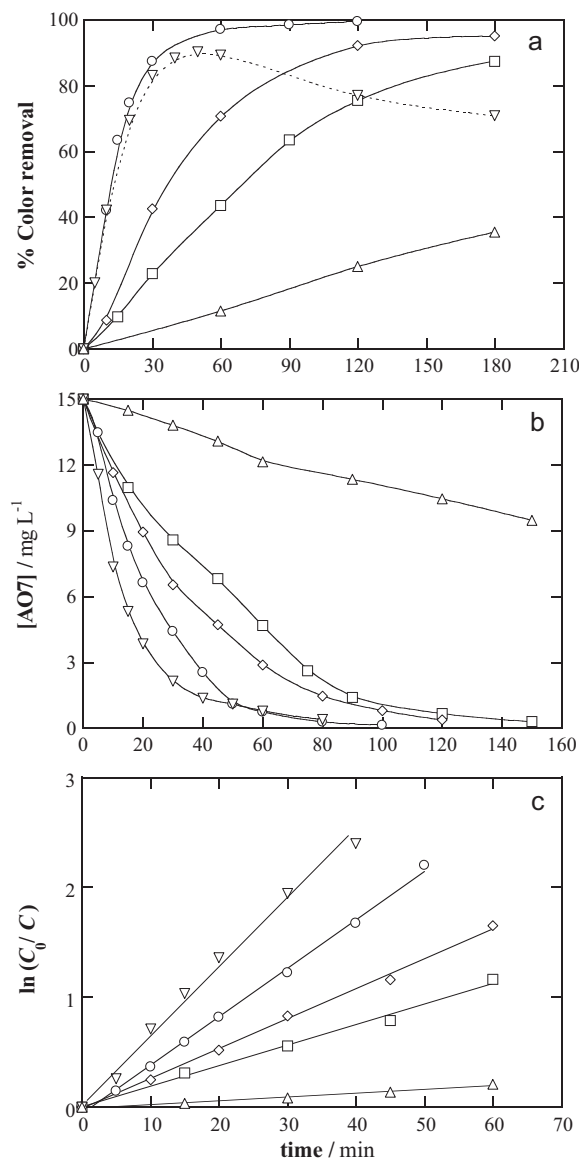


**Fig. 7.** Effect of anodic current density on (a) the percentage of color removal and (b) the dye concentration decay determined by reversed-phase HPLC with time for the treatment of 100 mL of a  $15 \text{ mg L}^{-1}$  AO7 solution in 0.05 M Na<sub>2</sub>SO<sub>4</sub> at pH 7.0 and 35 °C. (△) SPC and SPEC at  $j_{\text{anod}}$ : (□)  $0.25 \text{ mA cm}^{-2}$ , (◇)  $0.50 \text{ mA cm}^{-2}$ , (○)  $1.0 \text{ mA cm}^{-2}$  and (▽)  $2.0 \text{ mA cm}^{-2}$ . In plot (c), kinetic analysis of data given in plot (b) assuming that AO7 verifies a pseudo-first-order reaction.

optimum pH 7.0. Fig. 7a shows that a  $j_{\text{anod}}$  as low as  $0.25 \text{ mA cm}^{-2}$  already enhanced strongly the decolorization efficiency of the solution compared with that of the SPC process, as expected if the transport of photoelectrons to the cathode allows the fast generation of oxidant •OH from holes by reaction (2) [33–35]. Fig. 7a also evidences that the increase in  $j_{\text{anod}}$  from 0.25 to  $1.0 \text{ mA cm}^{-2}$  caused a quicker color removal owing to a faster electron-hole separation at the TiO<sub>2</sub> photoanode, as well as a faster oxidation of water from reaction (13), giving rise to higher •OH production, which is able to completely decolorize the solution after 120 min of electrolysis at  $1.0 \text{ mA cm}^{-2}$ . For  $2.0 \text{ mA cm}^{-2}$ , however, a decay in color removal can be observed after 50 min of SPEC treatment when 90% decolorization was already reached. This is due to the existence of an increasing residual absorbance in the visible region of the UV-vis spectrum of the solution, suggesting that the generation of an excess of oxidant •OH with a higher decrease of the local pH in the vicinity of the TiO<sub>2</sub> electrode at  $2.0 \text{ mA cm}^{-2}$  favors



the formation of colored aromatic intermediates. Unfortunately, these compounds could not be identified by reversed-phase HPLC. Consequently,  $1.0 \text{ mA cm}^{-2}$  is the best  $j_{\text{anod}}$  needed to decolorize the optimized AO7 solution in SPEC.

The decay kinetics for AO7 in the above trials was followed by reversed-phase HPLC, where it displayed a well-defined peak with retention time ( $t_r$ ) of 7.6 min. Fig. 7b shows that while the azo dye was very slowly removed by SPC, it was quickly destroyed by SPEC, much more rapidly with increasing  $j_{\text{anod}}$  from  $0.25$  to  $2.0 \text{ mA cm}^{-2}$ . Thus, AO7 was only reduced by 36% after 150 min of SPC, but disappeared in decreasing times of 150, 120, 100 and 80 min for increasing current densities of  $0.25$ ,  $0.50$ ,  $1.0$  and  $2.0 \text{ mA cm}^{-2}$ . This trend agrees with the expected larger production of oxidizing species (mainly  $\bullet\text{OH}$ ) when  $j_{\text{anod}}$  rises due to the faster separation of photogenerated holes and electrons on the  $\text{TiO}_2$  photoanode and the quicker anodic oxidation of water. Comparison of Figs. 7a and 7b evidences that the decolorization process in SPEC is always slower than AO7 decay, as expected if colored aromatic intermediates that absorb at  $\lambda = 484 \text{ nm}$  are formed during its degradation.

The concentration decays of Fig. 7b were analyzed using kinetic equations related to simple reaction orders and excellent linear correlations were only found for a pseudo-first-order reaction, as illustrated in Fig. 7c. From this analysis, increasing pseudo rate constants ( $k_{\text{SPEC}}$ ) of  $3.1 \times 10^{-4} \text{ s}^{-1}$  ( $R^2 = 0.993$ ) at  $0.25 \text{ mA cm}^{-2}$ ,  $4.5 \times 10^{-4} \text{ s}^{-1}$  ( $R^2 = 0.997$ ) at  $0.50 \text{ mA cm}^{-2}$ ,  $7.4 \times 10^{-4} \text{ s}^{-1}$  ( $R^2 = 0.993$ ) at  $1.0 \text{ mA cm}^{-2}$  and  $1.0 \times 10^{-3} \text{ s}^{-1}$  ( $R^2 = 0.992$ ) at  $2.0 \text{ mA cm}^{-2}$  were determined for the SPEC process, which were, as expected, much greater than the pseudo rate constant ( $k_{\text{SPC}}$ ) of  $5.8 \times 10^{-5} \text{ s}^{-1}$  ( $R^2 = 0.982$ ) obtained for SPC. This behavior suggests a constant production of oxidizing agents (mainly photogenerated holes and  $\bullet\text{OH}$ ) in both SPC and SPEC treatments. Taking into account the above  $k_{\text{SPEC}}$  and  $k_{\text{SPC}}$  values, the extent of the electrochemical enhancement ( $E$ , in %) was estimated from the following expression [33]:

$$E = \frac{k_{\text{SPEC}} - k_{\text{SPC}}}{k_{\text{SPEC}}} 100 \quad (15)$$

Very high values for  $E$  were thus obtained, which increased gradually in 81%, 87%, 92% and 94% with increasing  $j_{\text{anod}}$  values of  $0.25$ ,  $0.50$ ,  $1.0$  and  $2.0 \text{ mA cm}^{-2}$ . This confirms the relevant role of  $j_{\text{anod}}$  in SPEC to accelerate the production of oxidants.

### 3.6. AO7 mineralization and identification and evolution of generated carboxylic acid and released inorganic nitrogen ions

The  $15 \text{ mg L}^{-1}$  azo dye solution in  $0.05 \text{ M Na}_2\text{SO}_4$  of pH 7.0 was slowly mineralized in the  $\text{TiO}_2$ /air-diffusion photoelectrochemical cell under SPEC at  $j_{\text{anod}} = 1.0 \text{ mA cm}^{-2}$ . In these optimized conditions, the initial TOC of  $8.22 \text{ mg L}^{-1}$  was only reduced to  $4.93 \text{ mg L}^{-1}$  in 240 min, corresponding to 40% of mineralization. That means that although AO7 is completely removed in 100 min (see Fig. 7b), it forms more recalcitrant by-products that react very hardly with  $\bullet\text{OH}$ . It is expected the formation of the same kind of by-products by SPEC and SPC because the same oxidizing agents act in both system. However, the larger production of photogenerated holes and  $\bullet\text{OH}$  in the former treatment accelerates strongly the destruction of intermediates affecting their distribution in relation to the second one.

Ion-exclusion chromatograms of the above treated solution displayed well-defined peaks ascribed to carboxylic acids such as tartaric ( $t_r = 8.51 \text{ min}$ ), oxamic ( $t_r = 9.41 \text{ min}$ ), succinic ( $t_r = 11.7 \text{ min}$ ), acetic ( $t_r = 14.9 \text{ min}$ ) and phthalic acid ( $t_r = 27.7 \text{ min}$ ). Tartaric, succinic and acetic acids can be formed from the cleavage of the benzene ring of aromatic intermediates [2,50], whereas oxamic acid is expected to be produced from the degradation of  $N$ -derivatives. Phthalic acid is an aromatic dicarboxylic acid

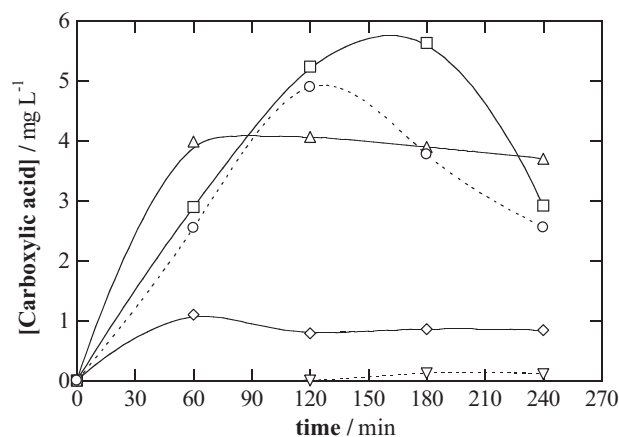


Fig. 8. Time-course of the concentration of: (○) phthalic, (□) tartaric, (△) succinic, (◇) acetic and (▽) oxamic acids detected during the SPEC degradation of 100 mL of a  $15 \text{ mg L}^{-1}$  AO7 solution in  $0.05 \text{ M Na}_2\text{SO}_4$  at pH 7.0 and  $j_{\text{anod}} = 1.0 \text{ mA cm}^{-2}$  and  $35^\circ\text{C}$ .

coming from the oxidation of the naphthalene moiety. Note that this latter by-product and succinic acid have also been detected in the degradation of AO7 by SPC with  $\text{TiO}_2$  in suspension [16].

Fig. 8 highlights that most carboxylic acids, except oxamic acid, were formed from the beginning of the SPEC treatment and attained their maximum content at about 120 min of electrolysis. At longer times up to 240 min, tartaric acid decayed from  $5.63$  to  $2.90 \text{ mg L}^{-1}$  and phthalic acid dropped from  $4.89$  to  $2.56 \text{ mg L}^{-1}$ , whereas succinic and acetic acids remained with contents practically constants near  $3.70$  and  $0.84 \text{ mg L}^{-1}$ , respectively. In contrast, oxamic acid only reached  $0.11 \text{ mg L}^{-1}$  at the end of SPEC, being detected for times  $> 120 \text{ min}$ . A simple mass balance of carboxylic acids accumulated at 240 min revealed that they account for by  $4.23 \text{ mg L}^{-1}$  TOC, i.e. 86% of the TOC contained in the remaining solution ( $4.93 \text{ mg L}^{-1}$ ). This indicates that the detected carboxylic acids are the main components of the final treated solution, which contains other minority unidentified organics only related to 14% of its TOC. Results of Fig. 8 corroborate the low ability of  $\bullet\text{OH}$  produced in the SPEC process to remove the recalcitrant carboxylic acids generated, thereby explaining the low mineralization of the AO7 solution in this treatment.

Ionic chromatograms of the electrolyzed solutions revealed the release of  $\text{NH}_4^+$  and  $\text{NO}_3^-$  ions in the mineralization of the initial N contained in AO7 ( $1.20 \text{ mg L}^{-1}$ ). No other inorganic nitrogen ions, like  $\text{NO}_2^-$  ion, were detected by this technique. After 240 min of SPEC,  $0.16 \text{ mg L}^{-1}$  of  $\text{NH}_4^+$  ion (10.4% of initial N) and  $0.54 \text{ mg L}^{-1}$  of  $\text{NO}_3^-$  ion (1.0% of initial N) were found, indicating that the former ion was produced in larger proportion. The TN analysis of this solution evidenced that it only contained  $0.23 \text{ mg L}^{-1}$  of N, corresponding to 19.2% of initial N. This suggests that during AO7 degradation in SPEC, the major part of its N (80.8%) is loss as volatile derivatives, probably  $\text{N}_2$  and  $\text{NO}_x$  species. Taking into account that  $\text{NH}_4^+$  and  $\text{NO}_3^-$  ions, as well as  $0.11 \text{ mg L}^{-1}$  of oxamic acid (1.4% of initial N), are detected as  $N$ -compounds in the final solution, one can concluded that 6.4% of initial N is retained in it in other recalcitrant unidentified  $N$ -derivatives.

## 4. Conclusions

It has been demonstrated that a novel  $\text{TiO}_2$  photoanode synthesized by APS can decolorize efficiently solutions with low contents of AO7 azo dye and  $0.05 \text{ M Na}_2\text{SO}_4$  using SPEC under direct sunlight irradiation in a photoelectrochemical cell with an air-diffusion cathode that generates  $\text{H}_2\text{O}_2$ . The photoanode presented excellent mechanical properties and showed large stability and long



durability up to  $2.0 \text{ mA cm}^{-2}$ . The SPEC process was synergistic of individual SPC and  $\text{AO-H}_2\text{O}_2$  ones under comparable conditions as a result of the larger production of  $\bullet\text{OH}$  from the higher amounts of photogenerated holes that can be separated of photogenerated electrons. Colored aromatic intermediates were formed in SPEC depending on pH, azo dye content and applied  $j_{\text{anod}}$ . The best operating variables were  $15 \text{ mg L}^{-1}$  AO7, pH 7.0 and  $j_{\text{anod}} = 1.0 \text{ mA cm}^{-2}$ . Under these conditions, the azo dye disappeared in 100 min and the solution was completely decolorized in 120 min, but its TOC was much more slowly removed only attaining 40% mineralization after 240 min of electrolysis. The AO7 decay followed a pseudo-first-order reaction, which was accelerated with increasing  $j_{\text{anod}}$  due to the higher  $\bullet\text{OH}$  generation from the production of more photogenerated holes and the faster anodic oxidation of water. Detected carboxylic acids like phthalic, tartaric, succinic, acetic and oxamic accounted for 86% of the TOC contained in the solution electrolyzed for 240 min and their large persistence explains the low mineralization degree achieved for the azo dye in SPEC. The initial N of AO7 was mineralized as  $\text{NH}_4^+$  ion and in a smaller proportion of  $\text{NO}_3^-$  ion, although it was mainly loss as volatile species. These results point to the use of SPEC followed by a biological treatment for the remediation of waters containing AO7, because the latter method can efficiently remove the large amounts of carboxylic acids formed from the application of the former one, thereby strongly increasing the mineralization degree of the azo dye.

## Acknowledgements

The authors thank the financial support from MICINN (Ministerio de Ciencia e Innovación, Spain) through project CTQ 2010-16164/BQU, co-financed with Feder funds, and from AGAUR (Agència de Gestió d'Ajuts Universitaris i de Recerca, Generalitat de Catalunya, Spain) through project 2009 SGR 00390. The grant awarded to S. Garcia-Segura by MEC (Ministerio de Educación y Ciencia, Spain) is also acknowledged.

## References

- [1] E. Forgacs, T. Cserhádi, G. Oros, *Environment International* 30 (2004) 953–971.
- [2] C.A. Martínez-Huitle, E. Brillas, *Applied Catalysis B: Environmental* 87 (2009) 105–145.
- [3] T. Robinson, G. McMullan, R. Marchant, P. Nigam, *Bioresource Technology* 77 (2001) 241–255.
- [4] G.A. Umbuzeiro, H.S. Freeman, S.H. Warren, D.P. Oliveira, Y. Terão, T. Watanabe, L.D. Claxton, *Chemosphere* 60 (2005) 55–64.
- [5] S.M.A.G. Ulson de Souza, E. Forgiarini, A.A. Ulson de Souza, *Journal of Hazardous Materials* 147 (2007) 1073–1078.
- [6] K.P. Sharma, S. Sharma, S. Sharma, P.K. Singh, S. Kumar, R. Grover, P.K. Sharma, *Chemosphere* 69 (2007) 48–54.
- [7] A. Szygula, E. Guibal, M. Ruiz, A.M. Sastre, *Colloids and Surfaces A* 330 (2008) 219–226.
- [8] M.M. Dávila-Jiménez, M.P. Elizalde-González, A.A. Pelaéz-Cid, *Colloids and Surfaces A* 254 (2005) 107–114.
- [9] J. Wu, C. Liu, K.H. Chu, S. Suen, *Journal of Membrane Science* 309 (2008) 239–245.
- [10] E. Franciscon, A. Zille, F. Dias Guimaro, C. Ragagnin de Menezes, L.R. Durrant, A. Cavaco-Paulo, *International Biodeterioration and Biodegradation* 63 (2009) 280–288.
- [11] T.A. Özbelge, F. Erol, *Chemical Engineering Communications* 169 (2008) 39–55.
- [12] R. Andreozzi, V. Caprio, A. Insola, R. Marotta, *Catalysis Today* 53 (1999) 51–59.
- [13] E. Brillas, J.C. Calpe, P.L. Cabot, *Applied Catalysis B: Environmental* 46 (2003) 381–391.
- [14] M. Pera-Titus, V. García-Molina, M.A. Baños, J. Giménez, S. Esplugas, *Applied Catalysis B: Environmental* 47 (2004) 219–256.
- [15] F. Kiriakidou, D.I. Kondarides, X.E. Verykios, *Catalysis Today* 54 (1999) 119–130.
- [16] M. Styliadi, D.I. Kondarides, X.E. Verykios, *Applied Catalysis B: Environmental* 40 (2003) 271–286.
- [17] S. Malato, J. Blanco, D.C. Alarcón, M.I. Maldonado, P. Fernández-Ibañez, W. Gernjak, *Catalysis Today* 122 (2007) 137–149.
- [18] A. Fujishima, X. Zhang, D.A. Tryk, *Surface Science Reports* 63 (2008) 515–582.
- [19] U.G. Akpan, B.H. Hameed, *Journal of Hazardous Materials* 170 (2009) 520–529.
- [20] R. Pourata, A.R. Khataee, S. Aber, N. Daneshvar, *Desalination* 249 (2009) 301–307.
- [21] D. Friedmann, C. Mendive, D. Bahnemann, *Applied Catalysis B: Environmental* 99 (2010) 398–406.
- [22] A.Y. Shan, T.I.M. Ghazi, S.A. Rashid, *Applied Catalysis A: General* 389 (2010) 1–8.
- [23] L.A. Ioannou, E. Hapeshi, M.I. Vasquez, D. Mantzavinos, D. Fatta-Kassinos, *Solar Energy* 85 (2011) 1915–1926.
- [24] J.H.O.S. Pereira, V.J.P. Vilar, M.T. Borges, O. González, S. Esplugas, R.A.R. Boaventura, *Solar Energy* 85 (2011) 2732–2740.
- [25] V.M. Daskalaki, Z. Frontistis, D. Mantzavinos, A. Katsounis, *Catalysis Today* 161 (2011) 110–114.
- [26] W.H. Leng, Z. Zhang, J.Q. Zhang, *Journal of Molecular Catalysis A: Chemical* 206 (2003) 239–252.
- [27] P.A. Carneiro, M.E. Osugi, J.J. Sene, M.A. Anderson, M.V.B. Zanon, *Electrochimica Acta* 49 (2004) 3807–3820.
- [28] M.G. Neelavannan, C.A. Basha, *Separation and Purification Technology* 61 (2008) 168–174.
- [29] K. Esquivel, L.G. Arriaga, F.J. Rodríguez, L. Martínez, L.A. Godínez, *Water Research* 43 (2009) 3593–3603.
- [30] J. Marugán, P. Christensen, T. Egerton, H. Purnama, *Applied Catalysis B: Environmental* 89 (2009) 273–283.
- [31] P.S. Shinde, P.S. Patil, P.N. Bhosale, A. Brueger, G. Nauer, M. Neumann-Spallart, C.H. Bhosale, *Applied Catalysis B: Environmental* 89 (2009) 288–294.
- [32] H.G. Oliveira, D.C. Nery, C. Longo, *Applied Catalysis B: Environmental* 93 (2010) 205–211.
- [33] Z. Frontistis, V.M. Daskalaki, A. Katsounis, I. Poulis, D. Mantzavinos, *Water Research* 45 (2011) 2996–3004.
- [34] R. Daghrir, P. Drogui, I. Ka, M.A. El Khakani, *Journal of Hazardous Materials* 199–200 (2012) 15–24.
- [35] R. Daghrir, P. Drogui, D. Robert, *Journal of Photochemistry and Photobiology A: Chemistry* 238 (2012) 41–52.
- [36] L. Yu, Z. Wang, L. Shi, S. Yuan, Y. Zhao, J. Fang, W. Deng, *Applied Catalysis B: Environmental* 113–114 (2012) 318–325.
- [37] S. Dosta, I.G. Cano, J.R. Miguel, J.M. Guilemany, *Journal of Thermal Spray Technology* 17 (2008) 360–364.
- [38] J. Suffner, H. Hahn, S. Dosta, I.G. Cano, J.M. Guilemany, *Surface and Coatings Technology* 204 (2009) 149–156.
- [39] J. Suffner, H. Sieger, H. Hahn, S. Dosta, I.G. Cano, J.M. Guilemany, P. Klimczyk, L. Jaworska, *Materials Science and Engineering A* 506 (2009) 180–186.
- [40] S. Ammar, R. Abdelhedi, C. Flox, C. Arias, E. Brillas, *Environmental Chemistry Letters* 4 (2006) 229–233.
- [41] L.C. Almeida, S. Garcia-Segura, N. Bocchi, E. Brillas, *Applied Catalysis B: Environmental* 103 (2011) 21–30.
- [42] E.J. Ruiz, C. Arias, E. Brillas, A. Hernández-Ramírez, J.M. Peralta-Hernández, *Chemosphere* 82 (2011) 495–501.
- [43] S. Garcia-Segura, F. Centellas, C. Arias, J.A. Garrido, R.M. Rodríguez, P.L. Cabot, E. Brillas, *Electrochimica Acta* 58 (2011) 303–311.
- [44] E. Brillas, M.A. Baños, S. Camps, C. Arias, P.L. Cabot, J.A. Garrido, R.M. Rodríguez, *New Journal of Chemistry* 28 (2004) 314–322.
- [45] F.H. Chung, *Journal of Applied Crystallography* 7 (1974) 519–525.
- [46] F.J. Welcher (Ed.), *Standard Methods of Chemical Analysis*, vol. 2, Part B, 6th ed, R.E. Krieger Publishers Co., Huntington, New York, 1975, p. 1827.
- [47] R. Restori, D. Schwarzenbach, J.R. Schneider, *Acta Crystallographica* 43B (1987) 251–257.
- [48] E. Sánchez, T. López, R. Gómez, X. Bokhimi, A. Morales, O.J. Novaro, *Journal of Solid State Chemistry* 122 (1996) 309–314.
- [49] Y. Le Page, P. Strobel, *Journal of Solid State Chemistry* 44 (1982) 273–281.
- [50] M. Panizza, G. Cerisola, *Chemical Reviews* 109 (2009) 6541–6569.